

## The Electron Optical Performance of the Gemini Lens Design for Low Voltage Scanning Electron Microscope

*M.A. Al-Khashab and N.S. Hujazie \**

### ABSTRACT

The superb resolution at low beam energies, down to 100 eV, is achieved by employing a compound lens which was used recently as an objective lens in low-voltage SEM, called Gemini lens.

A new program has been devised in FORTRAN language in order to compute the objective focal properties for the compound lens. It has been noticed that an improvement is achieved in the objective focal properties, especially at low beam energies, such as the aberration coefficients. The aberration coefficients achieved by our compound lens at beam voltage of 100 V are found to be lower than those achieved by pure magnetic lens by a factor of almost half. (i.e.  $C_s = 1.15$  mm,  $C_c = 0.78$  mm,  $W. D = 4$  mm and  $\delta \approx 10$  nm).

The results of the compound lens of our preferable design were compared with the results in the available published papers and found to be in good agreement over a wide range of applied voltage.

**Keywords:** Compound Lens, Gemini Objective Lens, Ultra-High Performance Objective Lens, Low-Voltage Scanning Electron Microscope (SEM).

### 1. INTRODUCTION

The low energy-range operation is employed in the scanning electron microscope (SEM) during the last two decades for many reasons. The reduced charging of the non-conductive specimen and better visualization of the surface relief were two of those reasons. The energy of around 1keV is available in the conventional SEM design. However, energy extension down to 100 eV was only possible while using a compound objective lens with a retarding field element [(Martin et al., 1995) and (Mika et al., 2003)]. The configuration of the compound lens (consists of the magnetic lens with an electrostatic immersion lens placed behind the specimen called Gemini objective lens ) was firstly applied by Frosien (Frosien et al., 1989) and then by Yonezawa (Yonezawa et al., 2002). Recently, a single pole piece lens was manufactured lens by Mohammed as a compound lens (Mohammed, 2010). Due to this combination design, the aberration coefficients were reduced by decreasing the

electron beam energy.

The low-voltage operation of the (SEM) was achieved in 1968 by employing Pease's principle (Paden and Nixon, 1968). It was found out that an electrostatic retarding field presented in front of the specimen can further improve the optical performance of the pure magnetic design. Other insignificant scheme, has been reported, in which the electrons are initially accelerated to a high potential ( $\sim 25$  keV) and then retarded to the desired energy by an electrostatic field presented just in front of the specimen (Meyer and Braun, 2008 ).

Many SEM's producers offer instruments nowadays with low resolution (several nm) at low energy (200-500) eV (Nagatani et al., 1990) and (Pawley, 1997). A high performance SEM's from Carl Zeiss, which has been developed under license to ICT GmbH (Kennedy et al., 2005) and (Drexel et al., 1994), offers resolution data that are not attained before, especially at low beam energies. The resolution for DSM 982 Gemini SEM was 1.2 nm at 20 keV, 2.5 nm at 5 keV and 4 nm at 1 keV (Martin et al., 1995). LEO 982 FESEM can also operate at an accelerating voltage ranging from 0.2 kV to 30 kV and has the resolutions of  $\geq 4$  nm at 1 kV and  $\geq 1$  nm at 30 kV (Young, 2004).

---

\* Department of Physics, College of Science and Basic Sciences Branch, College of Agriculture and Forestry, University of Mosul, Iraq. Received on 7/9/2010 and Accepted for Publication on 20/12/2010.

The combination of the magnetic and electrostatic technique opened a new area of applications. They used, for example, a new cross beam inspection tool combining an ultra high resolution field emission SEM with high resolution focused ion beam FIB (Gnauck et al., 2003).

The present paper tackles the lens design, optical properties and tests the performance of this class of compound lenses. However, an efficient program named (NED) has been developed for computing the trajectory of the electrons beam inside the structure of the compound lens. The properties of the combination of the magnetic and electrostatic focusing system are computed, too.

The principal aim of this work is to achieve an improved design for the new type of the electron lenses (compound lens), having an overlapping of the magnetic and electrostatic retarding fields concentrated inside the lens corpse (Gemini lens). This lens is perfectly suitable as an objective lens for low-voltage SEM's. This lens gives superb resolution at low beam energies.

## 2. DESIGN OF THE COMPOUND (MAGNETIC-ELECTROSTATIC) LENS

One of the important requirements for low-voltage electron beam systems is to design the focusing system with low aberrations. An additional electrostatic retarding field lens, situated behind the main magnetic lens was found to reduce the aberrations. For this purpose, a combination of the magnetic lens M1 with axial gap which possesses preferable design, and an asymmetrical two-coaxial cylinder electrostatic lens with an external conical shape (E41) acquires good lens design as previously obtained by Abd-Hujazie (Abd-Hujazie, 2006). The inner electrode (I) of this electrostatic lens consists of the lower-end of the beam-booster or beam-accelerator (which directs the electrons beam through the optical column). However, the outer electrode (II) consists of a cap connected to the lower magnetic polepiece lens as shown in Fig.1. The electrostatic lens is located between the magnetic lens and the image plane (specimen position). The electron beam is accelerated to a high potential (greater than 8000 V) in the full length of the column. The primary electrons are retarded to the selected beam energy, which can be as low as 100 eV, for a small gap at the final end of the pole piece. It is necessary, for example, to retard the primary beam from the booster by 7900 eV in order to achieve a resulting beam landing energy of 100 eV.

The on-axis values for the axial magnetic flux density  $B_z$ , and the axial potential  $V_z$ , the magnetic lens M1 and electrostatic lens E41 are first determined by the aid of the (AMAG) and (E11) programs, respectively (Lencova', 1986) and (Munro, 1975). This is achieved by using the finite element method employing a (26x52) meshes size. It is important to note that, the total number of the fine meshes was chosen to be constant 18 mesh (at the polepiece region) as illustrated in Fig.2. The results for the axial magnetic flux density distribution ( $B_z$ ) for lens M1 at excitation  $NI=500A-t$  and axial potential distribution ( $V_z$ ) for lens E41 ( $V_I = 8000$  V and  $V_{II} = 100$  V) as taken from  $Z = -168$  mm to  $Z = 30$  mm are shown in Fig.3.

## 3. CALCULATION OF THE PARAXIAL RAY ELECTRON TRAJECTORY INSIDE THE COMPOUND LENS

The paraxial ray trajectory  $R(z)$  can now be computed by solving the paraxial ray equation for a combined magnetic and electrostatic fields as follows : (Hawkes, 1972).

$$R''(z) + \frac{V'_z}{2V_z} R'(z) + \left( \frac{V''_z}{4\sqrt{V_z}} + \frac{eB_z^2}{8mV_r} \right) R(z) = 0 \quad (1)$$

Where  $V_z, V'_z$  the axial potential and the first derivative of the axial potential at each interval, respectively.

This equation can be solved numerically by using a fourth order Runge-Kutta formula as given by the following :

$$R(z+h) = R(z) + (2v_1 + 4v_2 + 2v_3 + v_4)/6 \quad (2)$$

$$R'(z+h) = R'(z) + (2W_1 + 4W_2 + 2W_3 + W_4)/6 \quad (3)$$

where

$$v_1 = \frac{1}{2} h R'_n, \quad v_2 = \frac{1}{2} h (R'_n + W_1), \quad v_3 = h (R'_n + W_2),$$

$$v_4 = h (R'_n + W_3)$$

and

$$W_1 = \frac{1}{2} h \left[ -\frac{1}{2} \frac{V''_n}{V_n} R'_n - \left( \frac{1}{4} \frac{V''_n}{V_n} + \frac{eB_n^2}{8mV_r} \right) R_n \right]$$

$$W_2 = \frac{1}{2} h \left[ -\frac{1}{2} \frac{V''_m}{V_m} (R'_n + W_1) - \left\{ \frac{1}{4} \frac{V''_m}{V_m} + \frac{eB_m^2}{8mV_r} (R_n + v_1) \right\} \right]$$

$$W_3 = h \left[ -\frac{1}{2} \frac{V'_m}{V_m} (R'_n + W_2) - \left\{ \frac{1}{4} \frac{V''_m}{V_m} + \frac{eB_m^2}{8mV_r} (R_n + v_2) \right\} \right]$$

$$W_4 = h \left[ -\frac{1}{2} \frac{V'_{n+1}}{V_{n+1}} (R'_n + W_3) - \left\{ \frac{1}{4} \frac{V''_{n+1}}{V_{n+1}} + \frac{eB_{n+1}^2}{8mV_r} (R_n + v_3) \right\} \right]$$

where  $v_1, v_2, v_3, v_4, W_1, W_2, W_3$  and  $W_4$  the Runge-Kutta coefficients.  $V_m, V'_m$  and  $V''_m$  are the potential, first and second derivatives of the potential at the middle points of each interval, respectively. The above equations are written in subroutine called (RAY NED) to compute the trajectory of the electron inside the compound lens presented in the main program named NED (see Appendix 1).

**Table 1. Electron optical performance results obtained from the compound lens compared with those obtained from the magnetic lens using (NED) program at an immersion ratios of (80 and 16) at a constant excitation (NI = 500 A-t)**

Lens mode	$V_I$ (Volt)	$V_{II}$ (Volt)	$f$ (mm)	$C_s$ (mm)	$C_c$ (mm)	$Z_i$ (mm)	Immersion ratio $V_I/V_{II}$
Magnetic lens M1	6255	6255	25.43	82.87	22.43	8.56	1
	6548	6548	26.43	92.09	23.43	9.61	1
	7217	7217	28.75	115.75	25.72	11.00	1
	8000	8000	31.46	148.35	28.41	14.78	1
Compound (magnetic & electrostatic) lens	8000	100	11.31	0.92	0.7	8.56	80
	8000	500	17.92	2.15	1.36	9.61	16

**Table 2. The variation of the objective focal properties for the compound lens with the final beam voltage ( $V_I = 30000$  V) at image plane.**

Final beam voltage $V_{II}$ (Volt)	Immersion ratio $V_I/V_{II}$	Principal plane ( $Z_p$ ) (mm)	Image plane ( $Z_i$ ) (mm)	Equivalent focal length $f_{eq} = Z_i - Z_p$ (mm)	Spherical aberration $C_s$ (mm)	Chromatic aberration $C_c$ (mm)
25000	1.2	-9.79	13.74	23.54	35.71	23.7
15000	2.0	-7.88	13.14	21.01	29.98	18.06
10000	3.0	-6.26	12.55	18.81	24.29	14.03
5000	6.0	-2.67	11.66	14.23	12.79	7.31
1000	30.0	3.0	10.26	7.25	2.42	1.54
500	60.0	3.9	10.04	6.14	1.62	1.06
100	300.0	4.56	9.86	5.3	1.15	0.78

The results computed accordingly are shown in Fig.4. The paraxial ray trajectory  $R(z)$  of the electrons beam inside the structure of the compound lens is plotted as a function of the distance ( $z$ ). It is shown in Fig.4 that, as in the combined mode, the focusing mechanism is more complex. The paraxial trajectory  $R(z)$  is first refracted towards the axis by the effect of the convergent magnetic lens (region 1), then it is refracted slightly away by the

diverging electrostatic doublet (region 2) and finally focused by its converging part (region 3).

#### 4. CALCULATION OF THE OBJECTIVE FOCAL PROPERTIES OF THE COMPOUND LENS

This section, demonstrates the performance of this type of the compound lens and compares its focal properties with those of the purely magnetic lens M1. The

optical analogy shows that the compound objective lens is a strong lens, and it is equivalent to a triplet lens with principal plane ( $Z_p$ ) moved closely to the specimen. It possesses a shorter equivalent focal length ( $f_{eq}$ ) compared to the purely magnetic lens and consequently, smaller axial aberrations. The objective focal properties of the compound lens were computed by the aid of the program (NED). The results computed for the objective focal properties of the compound lens were compared with those of the magnetic lens at the immersion ratio  $V_I/V_{II}$  of (16 and 80) and  $NI=500A-t$ , (see Table 1). It shows that the electrostatic retarding field lens can produce very significant reduction in the aberration values. Therefore, the optical properties are improved remarkably and the aberration coefficients are approximately lowered by a factor of two compared to those values presented in our first investigation made for the magnetic lens, (see the upper part of table 1).

**Table 3. The values of  $d_p$  calculated as a function of the final beam voltage**

Final beam voltage (Volt)	Spot diameter ( $d_p$ ) ( $\mu m$ ) $\times 10^{-3}$
25000	1.237
15000	1.56
10000	1.82
5000	1.90
1000	2.00
500	2.76
100	10.17

#### 4.1 Variation of the Objective Focal Properties with the Beam Voltage

As the immersion ratio ( $V_I/V_{II}$ ) increases by decreasing the beam voltage at the specimen position ( $V_{II}$ ), the cardinal plane (principal plane  $Z_p$ ) of the compound objective lens moves from the magnetic lens towards the electrostatic lens (i.e. next to the specimen). This phenomena reduces effectively both the focal length and the chromatic aberration coefficient  $C_c$  which is generally proportional to the focal length of the objective lens. The reduction in chromatic aberration implies the use of a short working distance (W.D.). The variations of the objective focal properties with varying the beam voltage of the compound lens are summarized in Table 2. It was found that, due to this design of the combination of

a magnetic lens together with the electrostatic immersion lens, the aberration coefficients ( $C_s$  and  $C_c$ ) tend to decrease by decreasing the beam voltage. Therefore, it draws a superb resolution down to 100 eV. It is important to note that, these results, that are obtained by using program (NED), are in good agreement with those published by (Martin et al., 1995) and (Gnauck et al., 2003).

#### 4.2 Variation of Spot Diameter of the Probe with Final Beam Voltage

The image resolution at low beam energies, as it is mentioned in the previous section, is primarily governed by the electron probe size which is limited by the chromatic aberration disc according to the following equation (Müllerová, 1999):

$$d_p = d_c = C_c \frac{\Delta V}{V} \alpha \quad (4)$$

where  $\Delta V/V_r$  is the partial changing in the electron beam voltage,  $C_c$  is the chromatic aberration coefficient of the probe forming lens and  $\alpha$  is angle of convergence of the electron beam.

The calculated values for the probe spot diameter ( $d_p$ ), of the present work, takes the standard values ( $\Delta V=0.3V$ ,  $\alpha=8.7 \times 10^{-3}$  rad) from the reference (Gnauck et al., 2003), as reported in Table 3. It should be noticed that, a slight increase of diameter occurs while the beam voltage slightly decreases.

### 5. COMPARISON BETWEEN THE RESULTS OBTAINED BY THE COMPOUND LENS AND THAT OBTAINED BY THE MAGNETIC LENS OF IDENTICAL DIMENSIONS

The following sections demonstrates the performance of the compound lens compared with that of the purely magnetic lens at identical dimensions.

Fig. 5 compares the trajectory ray of the electron inside the asymmetrical magnetic lens and that for the compound lens as a function of ( $z$ ). The solid line shows the trajectory ray  $R(z)$  for the magnetic mode, while, the dotted line shows the trajectory ray  $R(z)$  in the combined magnetic-electrostatic mode. The focusing in the combined mode is more complex because this combination is equivalent to an optical triplet lens. It is clear from this figure that the dotted line is first refracted towards the axis by the convergent effect of the magnetic

lens and then refracted slightly away by the first divergent lens of the doublet electrostatic in order to be

finally focused by its convergent second lens.

**Table 4. Comparison between the optical properties of the compound lens (present work) and those of the published results (other researchers)**

Lens Type	Ref.	Optical Properties				Final beam energy eV
		$C_s$ (mm)	$C_c$ (mm)	W.D (mm)	$d_p$ (nm)	
Gemini lens	(Present work)	2.42	1.54	4	2.00	1000
		1.62	1.06	4	2.75	500
		1.15	0.78	4	10.17	100
Gemini lens	(Frosion, 1989)	3.7	1.8	4	11	500
Gemini lens	(Lencová, 1995)	5.0	2.3	-	-	1000
DSM 982	(Martin et al., 1995)	-	-	-	1.2	20000
Gemini	(Martin et al., 1995)	-	-	-	2.5	5000
		-	-	-	4.0	1000
Add-on immersion magnetic lens	(Khursheed and Karuppiah, 2002)	-	-	-	2.67	1000
		-	-	-	3.26	600

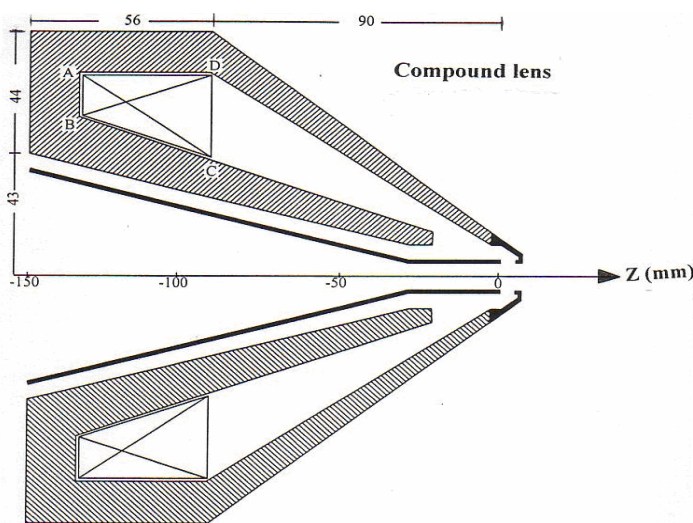


**Fig. 1. A schematic diagram for the compound lens (magnetic lens (M1) and electrostatic lens (E41))**

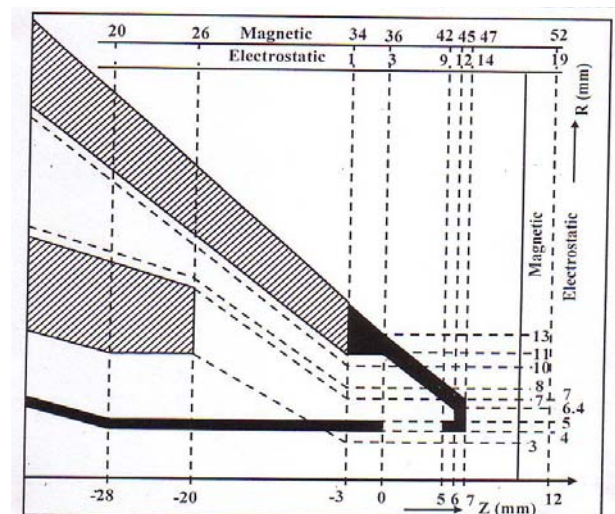


**Fig. 2. The finite element mesh specification for the compound Magnetic (M1) and electrostatic (E41) lenses with their corresponding radial (R) and axial (Z) dimensions**

In order to compare the electron optical properties of the preferred compound lens with that of the asymmetrical magnetic electron lens designed by the present work, the spherical and chromatic aberration coefficients of these lenses have been presented as a function of the final beam voltage at a constant working distance (W.D.=4mm) as displayed in Figure (6). It is noticed that the variation of  $C_s$  and  $C_c$  are independent of the final beam voltage in the magnetic lens (solid

lines). However the values of  $C_s$  and  $C_c$  decrease while the beam voltage decreases as in case of the combined mode (dotted lines). This shows a progressive improvement in both  $C_s$  and  $C_c$  due to the combination of magnetic and electrostatic retarding field lenses, especially at low beam voltage.

It is important to display the total spot diameter (resolution) as a function of the final beam voltage for the magnetic lens compared with that obtained for the

compound lens. The values calculated for the probe spot diameter ( $d_p$ ), by using the standard values ( $\Delta V = 0.3 \text{ V}$ ,  $\alpha = 8.7 \times 10^{-3} \text{ rad}$ ) for comparison purposes, are shown in Fig(7). The compound mode (dotted line) shows a slight increase in the diameter ( $d_p$ ) by decreasing the beam voltage. This phenomena is in contrast to that obtained for the magnetic lens (solid line) at identical

dimensions. The corresponding values of the magnetic lens are obtained by simply switching off the electrostatic retarding field. The direct comparison between both lenses demonstrates the outstanding features of the combined (magnetic and electrostatic) lens over the purely magnetic lens.

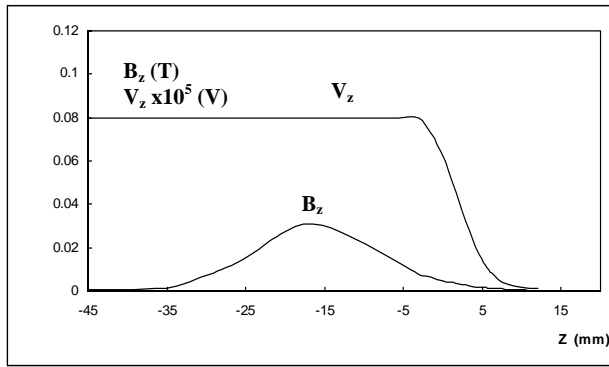


Fig. 3. The axial magnetic flux density distribution  $B_z$  for the magnetic lens M1 at excitation ( $NI=500 \text{ A-t}$ ) together with the axial potential distribution  $V_z$  for the electrostatic lens E41 at constant voltages ( $V_I = 8000 \text{ V}$  and  $V_{II}=100 \text{ V}$ )

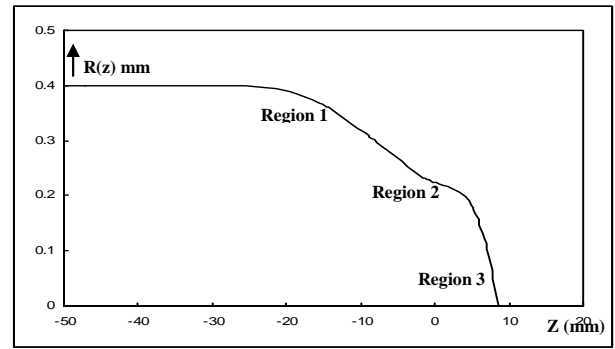


Fig. 4. The paraxial ray trajectory of the electrons beam  $R(z)$  inside the structure of the compound lens as a function of the distance ( $Z$ )

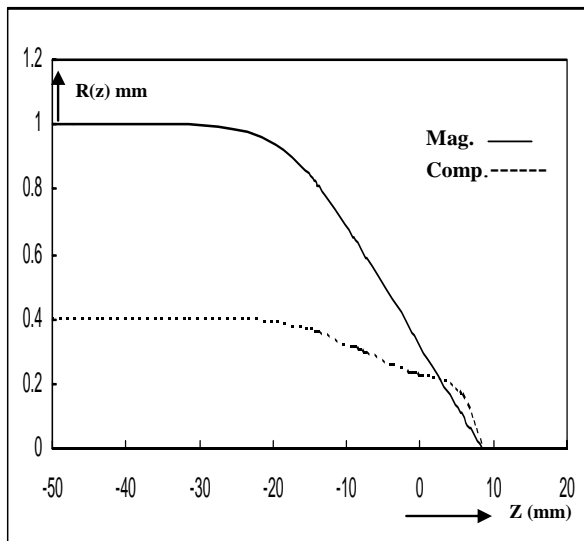


Figure 5. Comparison between the trajectory ray of the electron inside the purely magnetic lens (solid line) and that of the compound lens (dotted line) as a function of the distance ( $z$ )

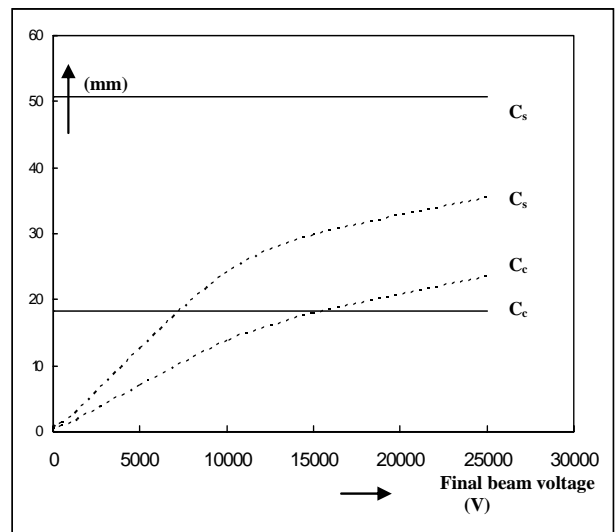
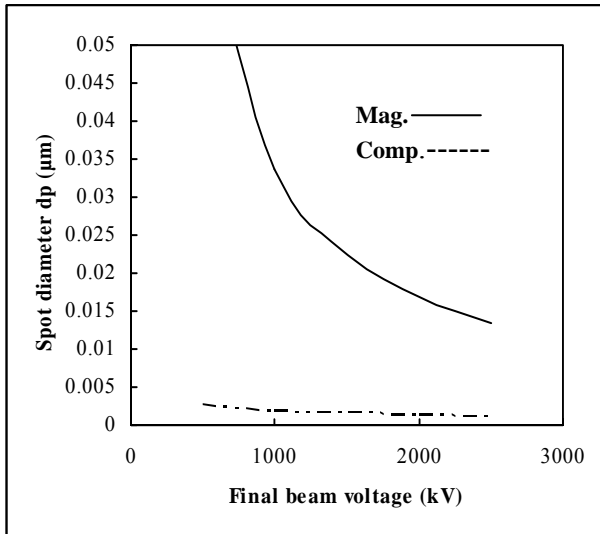


Figure 6. Comparison between the optical properties ( $C_s$ ,  $C_c$ ) of the purely magnetic lens (solid lines) and those of the compound lens (dotted lines) as a function of the final beam voltage at a constant value of the working distance ( $W.D.=4 \text{ mm}$ )

Table 4 shows the comparison between the objective focal properties of the compound lens of the present work and the results obtained from previously works.

The advantages of the Gemini lens design over the classical traditional lens may be summarize as follows:

The most important feature of the Gemini lens is to reduce the aberration coefficients ( $C_s$  and  $C_c$ ) by decreasing the beam voltage (or energy). Therefore, it produces superb resolution down to 100 eV. The Gemini lens design overcomes the shortage in the classical



**Fig. 7. Comparison between the values of probe spot diameter for the purely magnetic lens (solid line) and that obtained from the compound lens (dotted line) as a function of the final beam voltage**

objective lens designs that immerses the specimen in the magnetic field preventing imaging the magnetic samples. The Gemini lens was designed in certain shapes to minimize the magnetic field at the specimen. Therefore,

#### Appendix (I) SUBROUTINE RAYNED

```

SUBROUTINE
RAYNED(H,B,BM,T,TM,U,UM,NSTART,NFIN,VR,R
,S,NI)
IMPLICIT REAL*8(A-H, O-Z)
DIMENSION
B(1),BM(1),T(1),TM(1),U(1),UM(1),R(1),S(1)
ETA=1.7589E11
P=-ETA/(8.*VR)
G=0.5*H
NSTART=1
R(1)=0.4
S(1)=0.0
CALL SUBINT(B, BM, NI)
CALL SUBINT2(T, TM, NI)
CALL SUBINT2(U, UM, NI)
I=NSTART
1 A=P*B(I)*B(I)
C=P*BM(I)*BM(I)
D=P*B(I+1)*B(I+1)
V1=G*S(I)
W1=G*(-0.5*T(I)*S(I)-(0.25*U(I)-A)*R(I)

```

the high resolution of imaging the dia, para, or ferromagnetic samples was possible with very short working distance.

## 6. CONCLUSIONS

The analyses and calculations made for the two kinds of lenses show that the superposition of the magnetic and the electrostatic retarding fields produces an excellent electron optical lens compared to that for the purely magnetic lens. This combination provides a dramatic reduction in the aberration coefficients especially at low beam energies. In addition, this combination provides ultra-high image resolution at low beam voltage (2.75 nm spot size at 500 V beam voltage and 10.17 nm at 100 V, respectively). The variation of  $C_s$  and  $C_c$  are independent of the final beam voltage in a purely magnetic lens, while in the case of the combined mode, the values of  $C_s$  and  $C_c$  tend to decrease while the beam voltage decreases. This result is considered as one of the advantages of using this type of compound lens at low-voltage applications. Our program (NED) can handle any combination of the magnetic and the electrostatic lenses.

```

V2=G*(S(I)+W1)
W2=G*(-0.5*TM(I)*S(I)+W1)-(0.25*UM(I)-
C)*(R(I)+V1))
V3=H*(S(I)+W2)
W3=H*(-0.5*TM(I)*S(I)+W2)-(0.25*UM(I)-
C)*(R(I)+V2))
V4=H*(S(I)+W3)
W4=H*(-0.5*TM(I+1)*S(I)+W3)-(0.25*UM(I+1)-
D)*(R(I)+V3))
R(I+1)=R(I)+(2.0*V1+4.0*V2+2.0*V3+V4)/6.0
S(I+1)=S(I)+(2.0*W1+4.0*W2+2.0*W3+W4)/6.0
I=I+1
WRITE(18,5)I,R(I),S(I)
5 FORMAT(14,2F11.4)
IF(R(I))3,3,2
2 IF(I-NI)1,4,4
3 NFIN=I-1
RETURN
4 NFIN=NI
RETURN
END

```

## REFERENCES

- Abd-Hujazie, N.S. 2006. *Design of a Compound Lens (Magnetic- Electrostatic) for Low Voltage Scanning Electron Microscope*, Ph.D. Thesis, The University of Mosul, Iraq.
- Drexel ,V., Weimer, E., Martin, J.P. 1994. Ultra-high resolution column for the scanning electron microscope, Proc. MSA (Eds. Bailey GW, Garrett-Reed AJ). San Francisco press, 486-487.
- Frosien, J., Plies, E., Anger, K. 1989. Compound magnetic and electrostatic lenses for low-voltage applications, *J. Vac. Sci. Technol.*, B7 (6): 1874-1877.
- Gnauck, P., Hoffrogge, P., Greiser, J. 2003. A new cross beam inspection tool combining an ultrahigh resolution field emission SEM and a high resolution FIB, *Future Fab. Int 1.*, 15.
- Hawkes, P.W. 1972. *Electron optics and electron microscopy*, Taylor and Francis Ltd., London.
- Kennedy, M.S., Olson, A.L., Raupp, J.C. Moody, N.R., Bahr, D.F. 2005. Coupling bulge testing and nanoindentation to characterize materials properties of bulk micromachined structures, *Microsystem Technologies Springer-Verlag*, 298-302.
- Khursheed, A. and Karuppiyah, N. 2002. A high-resolution mixed field immersion lens attachment for conventional scanning electron microscopes, *Rev. Sci. Instrum.*, 73 (8): 2906-2909.
- Lencová, B. 1986. Program AMAG for computation of vector potential in rotationally symmetric magnetic electron lenses by FEM, *Inst. Sci. Brno, Czechoslovakia*, 1-58.
- Lencová, B. 1995. CAD in electron optics, *Proceeding Multinational Congress on Electron Microscopy*, Slovakia Academic Press, Bratislava, 19-24.
- Meyer, E., Braun, H.G. 2008. Micro-and nanomanipulation inside the SEM " Electron Microscopy and Analysis Group Conference (EMAG 2007), *Journal of Physics* : Conference Series 126.
- Martin, J. P. Drexel, V., Jaksch, H. and Weimer, E. 1995. New scanning electron microscope opens up new horizons in materials sciences, and biology DSM 982 Gemini, *Zeiss Information with Jena Review*, 4 (5): 14-16.
- Mika, F. Rysavka, J., Lopour, F. Zadrazil, M. Müllerová, I. and Frank, L. 2003. Computer controlled low energy SEM, *Microscope. Microanalysis*, 9 (3): 116-118.
- Mohammed, F.A. 2010. *Design chroma corrected objective compound lens for low beam energies for scanning electron microscope*, Ph.D. thesis, The University of Mosul, Iraq.
- Müllerová, I. 1999. Imaging of specimens at optimized low and very low energies in SEM, *Scanning Microscopy*, 13 (1): 7-22.
- Munro, E. 1975. A set of computer programs for calculating the properties of electron lenses, Cambridge University, Eng. Dept., Report CUED/B-ELECT/TR 45.
- Nagatani, T., Sato, M., Osumi, M. 1990. Development of an ultra high resolution low voltage (LV)SEM with an optimized "in-lens" design" Proc. XIIth ICEM Mtg seattle, 388-389.
- Paden, R.S. and Nixon, W.C. 1968. Retarding field Scanning electron microscope, *J. Sci. Instrum. (J. Phys. E.)*, 1 (11): Ser. 2, 1073-1080.
- Pawley, J. 1997. The development of field-emission scanning electron microscopy for imaging biological surfaces, *Scanning*, 19: 324-336.
- Yonezawa, A. Maruo, M. Takeuchi, T. Morita, S. Noguchi, A. Takaoka, O. Sato, M. and Wannberg, B. 2002. Single polepiece objective lens with electrostatic bipotential lens for SEM, *Journal of Electron Microscopy*, 51: 149-156.
- Young, J. 2004. LEO 982 field emission SEM, Anatine user facility for the scientific community [webmaster@ensi.poi.gov](mailto:webmaster@ensi.poi.gov)

**(Gemini Lens)**

\*

(100eV)

.(Gemini Lens)

100 V

10 nm

Cs=1.15 mm Cc=0.78 mm

.W.D.=4 mm

Gemini

:

---

\*

.2010/12/20

2010/9/7